

# Nanocrystal Diffusion in a Liquid Thin Film Observed by in Situ Transmission Electron Microscopy

Haimei Zheng,<sup>†,‡,§</sup> Shelley A. Claridge,<sup>§</sup> Andrew M. Minor,<sup>†,‡,||</sup>  
A. Paul Alivisatos,<sup>\*,†,§</sup> and Ulrich Dahmen<sup>\*,†,‡</sup>

*National Center for Electron Microscopy and Materials Sciences Division, Lawrence Berkeley National Laboratory, Berkeley, California 94720, and Department of Chemistry and Department of Materials Science and Engineering, University of California, Berkeley, California 94720*

Received April 18, 2009

## ABSTRACT

We have directly observed motion of inorganic nanoparticles during fluid evaporation using a transmission electron microscope. Tracking real-time diffusion of both spherical (5–15 nm) and rod-shaped (5 × 10 nm) gold nanocrystals in a thin film of water–15% glycerol reveals complex movements, such as rolling motions coupled to large-step movements and macroscopic violations of the Stokes–Einstein relation for diffusion. As drying patches form during the final stages of evaporation, particle motion is dominated by the nearby retracting liquid front.

When a liquid that contains colloidal nanoparticles evaporates from a surface, a variety of intricate patterns can form.<sup>1,2</sup> In a controlled drying process<sup>3,4</sup> large-scale arrays of highly organized patterns of nanoparticles can be generated. For example, capillary forces can overcome the random thermal fluctuations so that nanoparticles diffuse into prepatterned holes or templates on a substrate surface.<sup>4</sup> Controlled self-assembly of nanocrystals into functional patterns holds promise as a scalable fabrication strategy to systematically produce nanoscale devices. However, fluid deposition of nanoparticles is poorly understood and generally not predictable at the present time. One of the fundamental questions underlying particle assembly is what are the characteristics of the particle diffusion near surfaces and during the last moments before liquid drying?

As the thickness of a solution approaches the nanometer scale, several factors influence the particle motion. These include solvent surface fluctuations,<sup>2</sup> air–liquid\substrate–liquid interface structure<sup>4,5</sup> as well as the intrinsic differences in the relaxation and transport properties in an ultrathin liquid film compared to its bulk.<sup>6–9</sup> Diffusion of nanoparticles in such thin liquid films is largely beyond the predictive

capabilities of current theoretical computation.<sup>10</sup> The challenge for experimentalists is that it has not been possible to directly image the details of the dynamical diffusion processes in real time due to instrumental limitations.

By taking advantage of the high spatial resolution of a transmission electron microscope (TEM), we were able to observe the microscopic details of nanoparticle motion during fluid evaporation. Imaging of liquid samples using a TEM is achieved here by using a newly designed self-contained liquid cell (see details on the liquid cells in the Supporting Information and related techniques by Williamson et al.<sup>12</sup>). For imaging, about a hundred nanoliters of a dilute solution of Au nanoparticles in a water–glycerol mixture was loaded into one of the reservoirs in the liquid cell. The solution was dilute in order to avoid interactions between the gold particles for this work, although concentrated solutions could also be examined by this method (see liquid sample preparation in Supporting Information). Liquid solution was drawn from the reservoir into the window by capillary forces and formed a liquid layer confined between two electron transparent silicon nitride membranes. Subsequently, the liquid cell was sealed and loaded into a TEM as a standard TEM sample.

The liquid slowly evaporates inside the microscope due to the imperfect seal of the cell in a vacuum environment and a relative high vapor pressure of the liquid. Consequently, one side of the liquid film generally detaches from the silicon nitride membrane, creating a vapor–liquid interface. Observations are thus of particles moving in a thin liquid film between a solid substrate and a liquid–vapor

\* To whom correspondence should be addressed: alivis@berkeley.edu or udahmen@lbl.gov.

† National Center for Electron Microscopy, Lawrence Berkeley National Laboratory.

‡ Materials Sciences Division, Lawrence Berkeley National Laboratory.

§ Department of Chemistry, University of California.

|| Department of Materials Science and Engineering, University of California.

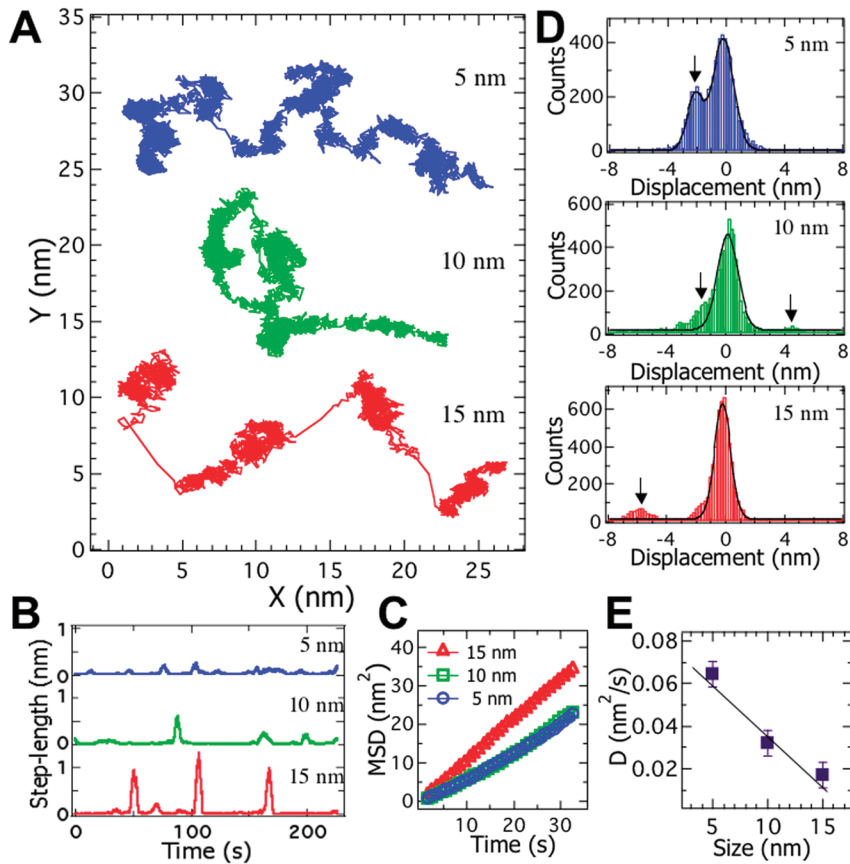


**Figure 1.** Analysis of different sized particle motion. (A) Trajectories of 5, 10, and 15 nm particle motion in the same liquid film recorded over the same time period of 233 s. Initial positions are arbitrary. (B) Displacements during a time interval of 6 s vs time. (C) Mean-square displacement, MSD, vs time. (D) Histograms showing the distributions of different sized particle displacements during a time interval of 6 s. Black curves show Gaussian fits. Additional peaks due to the larger step movements are marked by arrows. (E) Diffusion constants,  $D$ , due to the small-step movements only (corresponding to the main peak around zero displacement in histograms) vs particle size. Black line shows linear fit.

interface, as it would occur during most drying processes. Due to the slow evaporation rate of the fluid ( $\sim 1$  nm/min, see Supporting Information), our observations are of the particle motion in a liquid thin film with negligible changes in the film thickness.

We first study the nanoparticle motion before the formation of drying patches and when the liquid thickness is close to but greater than the nanoparticle diameter. Throughout this period, the nanoparticles execute a complex trajectory of motions which show significant effects from the substrate surface. From image analysis, we obtain data sets consisting of a particle's two-dimensional center-of-mass positions  $R(t_i) = [x(t_i), y(t_i)]$  in the lab frame with spatial resolution of 1 nm and temporal resolution of 30 ms. For asymmetric particles we also measure the orientation angles,  $\theta(t_i)$ , relative to the  $x$ -axis with resolution of  $1^\circ$  (Figure 3C). Microscopic details of the particle movement can be obtained from the individual video frames.

We have considered the effects that the electron beam might have on the particle motion, including local heating,<sup>12,13</sup> direct momentum transfer from the electron beam,<sup>12</sup> and electron charging.<sup>14</sup> In the water–glycerol mixture under study here, thermal fluctuations in the liquid are large compared to the energy imparted to the particles by the

electron beam. Thus, while an energetic electron beam such as that in the TEM can drive nanoparticle motion in some circumstances, such as on a dry substrate, this is not a significant consideration here, as the electron beam effects on particle motion is a few orders of magnitude smaller than the liquid thermal effects. It is also evidenced by the negligible differences in particle trajectories obtained at beam currents that differ by a factor of 5 (see the theoretical calculation and experiments in the Supporting Information).

Due to the complexity of a nonequilibrium liquid under evaporation, it is difficult to estimate the exact liquid conditions (e.g., liquid thickness, etc.), which makes it impractical to compare particle diffusion from different samples. In order to study the variation of particle motion as a function of nanoparticle size, we mixed nanoparticles of different sizes together and collected trajectories from particles of different sizes that were close to each other. Trajectories of two-dimensional particle displacement for three particles sizes, 5, 10, and 15 nm in diameter, in the same liquid film recorded in the same time period before drying patches initiated are shown in Figure 1A (also see movie S1 in Supporting Information). A liquid thickness of roughly 20–30 nm was estimated by assuming a linear evaporation rate.<sup>15</sup> The particle trajectories exhibit sparse and

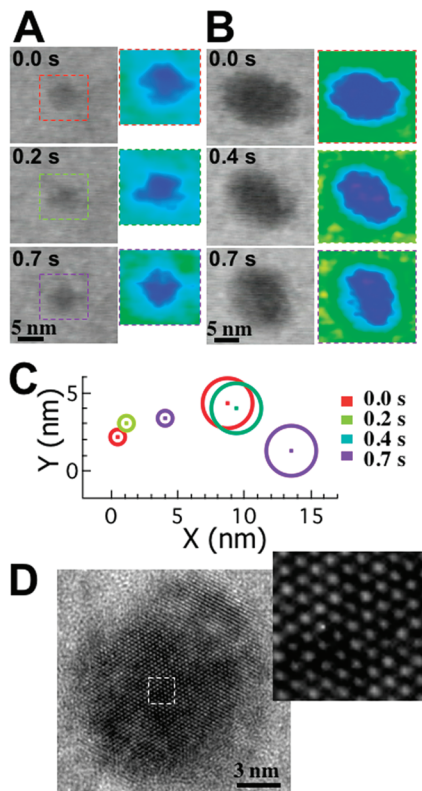


**Figure 2.** Jump motion corresponding to particle orientation changes. (A) An image sequence showing the orientation changes of a 5 nm particle during a jump. The orientation changes indicated by the difference in diffraction intensities within the particle are highlighted using color gradient maps. (B) An image sequence showing the orientation changes of a 15 nm particle during a jump. (C) Jump distances (center-of-mass displacements) of the 5 nm particle in (A) and 15 nm particle in (B) within a time interval of 0.7 s. (D) High-resolution TEM image of a gold particle inside the liquid cell after the diffusion experiment (the liquid has dried out). An enlarged view of the marked section is shown in the upper right. The original video images corresponding to (A) and (B) are provided in panels A and B of Figure S3 in Supporting Information.

larger step movements, which we term “jumps”, between swarms of much smaller steps. Larger jump distances were observed for larger particles. In order to quantify this behavior, we analyzed the particle displacement ( $\lambda$ ) during a time interval ( $\Delta t$ ) as a function time ( $t$ ), shown in Figure 1B (see detailed analysis in the Supporting Information and reference by Raptis et al.<sup>16</sup>). Particle jumps, corresponding to peaks in the plot in Figure 1B, are followed by an extended series of small-step displacements along the trajectory. There was no obvious correlation between the jumps of different, but nearby particles. Thus, we conclude that these jumps are not the result of large-scale liquid motion (for example, convection or turbulence), which would be similar for nearby particles within the small field of view (about  $100 \text{ nm}^2$ ). The mean-square displacement, MSD ( $\langle x^2 \rangle$ ), including all multiscale step movements is approximately linear with time ( $t$ ); see Figure 1E. This allows estimation of two-dimensional diffusion coefficients  $D = \langle x^2 \rangle / 4t$ , from which  $0.165 \text{ nm}^2/\text{s}$  for the 5 nm,  $0.172 \text{ nm}^2/\text{s}$  for the 10 nm, and  $0.268 \text{ nm}^2/\text{s}$  for the 15 nm particle were obtained. It is interesting to note that the larger diffusion coefficients observed for larger

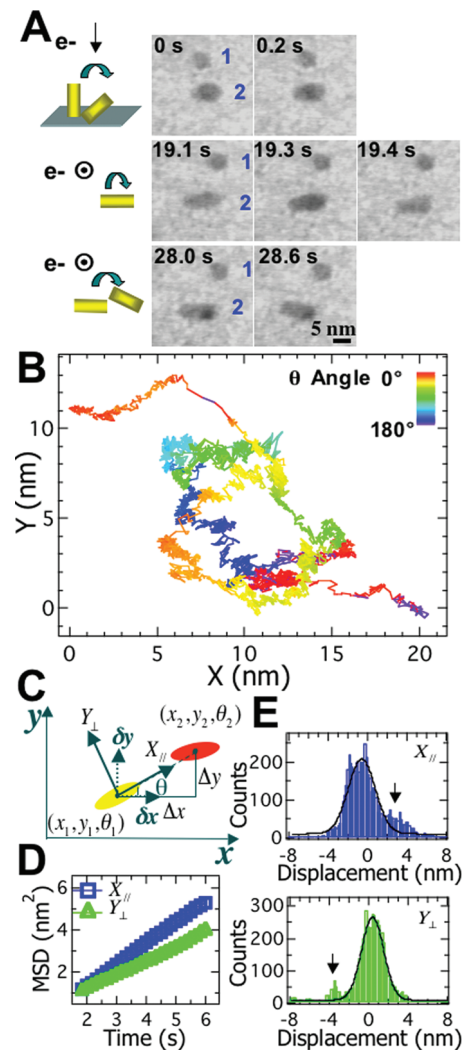


**Figure 3.** Asymmetric particle motion. (A) Selected image sequences showing a 510 nm asymmetric particle (particle 2) undergoing different types of motion: rotation from vertical to in-plane, rolling around its long-axis, and wagging. Particle 1 is a reference particle with no random motion. The direction of the electron beam ( $e^-$ ) is indicated by an arrow; a circle indicates that the beam is normal to the figure. (B) A trajectory of the rod-shaped particle’s 5550-step center-of-mass displacements in a liquid thin film. Each step is  $1/30 \text{ s}$ . Orientations are labeled with a rainbow color scale. (C) Particle motion can be referred to the body frame ( $X_{||}, Y_{\perp}$ ) or the lab frame ( $x, y, \theta$ ). (D) Mean-square displacement, MSD, vs time showing the asymmetric motion along the axes. (E) Histograms showing the distributions of the particle displacements during a time interval of  $6 \text{ s}$  along the axes. Black curves show Gaussian fits. Additional peaks due to the larger step movements are marked by arrows.

particles violates the Stokes–Einstein relationship, in which  $D$  scales inversely with particle diameter.

Detailed characterization of the particle motion reveals the mechanism of this violation. The histograms of particle displacement distribution show multiple peaks corresponding to the different scales of step movements, namely, a main peak around zero displacement due to the small-step movements and subsidiary peaks due to the larger step movements (Figure 1D). The main peaks around zero displacement can be fit by Gaussian distributions. The standard deviation of the distribution represents the average step displacement during the time interval. A diffusion constant due to the

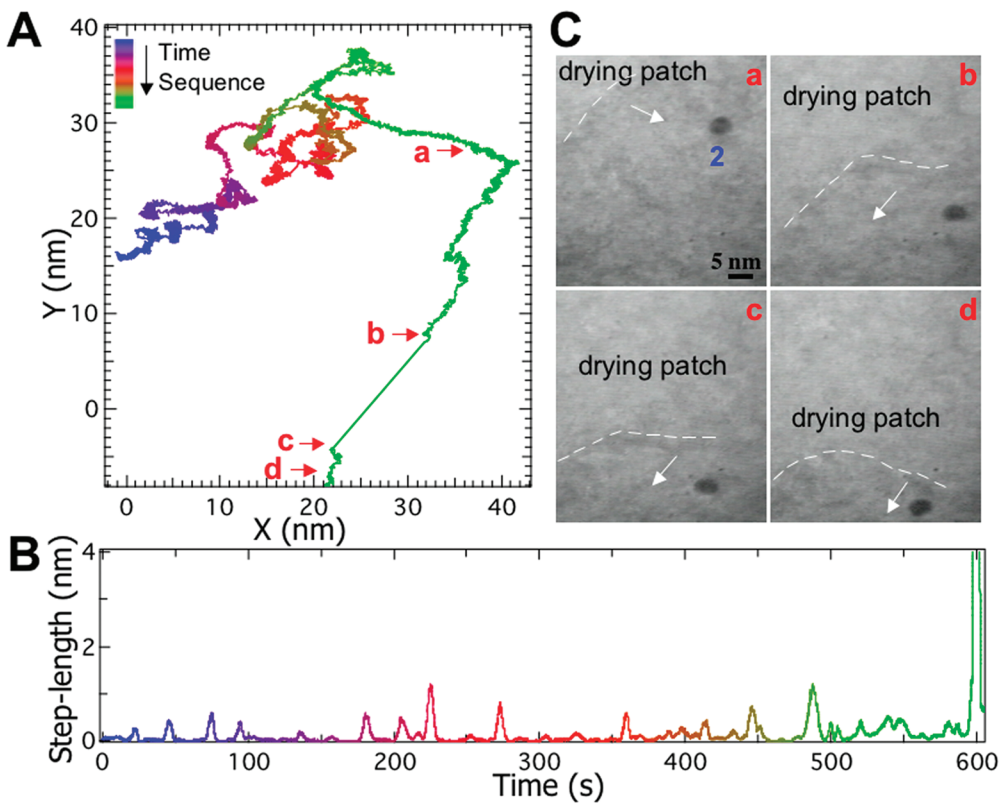


**Figure 4.** A 5 nm particle motion in a liquid thin film until the formation of drying patches. (A) Trajectory of 18150-step movement. Each step is 1/30 s. The initial position is arbitrary. The time variable is labeled with a rainbow color scale. (B) Displacement during a time interval of 2 s vs time. (C) An image sequence corresponding to the positions in the trajectory in (A) showing the particle being dragged by the nearby retracting liquid front at the later stage of solvent evaporation: a, 602.0 s; b, 665.9 s; c, 666.0 s; d, 671.6 s.

small-step movements only can be obtained from the average small-step displacement as a function of time. The diffusion constant due to the small-step movement is roughly inversely proportional to particle size; see Figure 1E. Therefore, the larger step jump diffusion is the main contribution to the violation of the Stokes–Einstein relationship.

Analysis of individual images indicates particle contrast changes during each jump (see parts A and B of Figure 2 as examples). However, the particle contrast mostly remains the same for the small-step movements (Figure S3C in Supporting Information). Since the particles are crystalline (Figure 2D), the contrast changes result from changes in particle orientation and the correspondingly different diffraction intensities.<sup>17</sup> It was observed that the particle rotates along the direction of movement (rolling) for the 15 nm particle. The rolling motion suggests a significant effect of the substrate surface on the particle movement.<sup>18,19</sup> Nanoparticles in solution can be weakly bound near the surface due to a potential for attraction between the surface and the particles.<sup>20</sup> Luedtke and Landman<sup>21</sup> predicted this type of anomalous diffusion behavior for nanoparticles near a dry surface about 10 years ago, but it has not been possible to directly observe this previously. In their model, the initiation of rolling is attributed to a thermal fluctuation overcoming the energy barrier of interaction between the substrate and the particle. The differences in our case are that the particles are in a thin film liquid and only limited rolling distances

were observed. Statistically, the step lengths consist roughly of two normal distributions (Figure 1D) instead of Lévy flight characteristics (a power law dependence of step length<sup>21–23</sup>). Experimentally, these two modes of particle motion can be classified as the motion in the liquid thin film and the motion confined on the substrate surface. There also might be additional factors (e.g., lateral capillary forces or local convective flow) from the liquid surface affecting the movement of the larger particles more strongly than the smaller particles.<sup>24</sup> In a thin liquid film, such effects can drive the larger particles to move faster than the smaller ones. We have found that the jumps of the largest particles are roughly along certain directions (Figure 1A), which suggests that the particles might be moving in the direction of local convective flow or are dragged by a lateral capillary force. Our observation is consistent with earlier studies on the size-dependent separation of colloidal nanoparticles during fluid evaporation.<sup>25,26</sup> However, direct observation of the size-dependent movement of individual nanoparticles during fluid evaporation has not been possible before.

Particle orientation changes correlated to particle jumps in the liquid film are more clearly seen in the motions of an asymmetric particle (5 × 10 nm). For example, rotation from vertical to in-plane and rolling around its long axis in addition to in-plane rotation and translation were observed; see Figure 3A and movie 2S in Supporting Information. The consecutive center-of-mass translational

motion and orientation are plotted in Figure 3B, in which orientations  $\theta$  relative to the  $x$ -axis are labeled with a rainbow color scale. A uniaxial anisotropic particle is characterized by parallel and transverse components of hydrodynamic friction coefficients,  $\gamma_{\parallel}$  and  $\gamma_{\perp}$ , respectively, for motion parallel to its long axis ( $X_{\parallel}$ ) and perpendicular to its long axis ( $Y_{\perp}$ ). In general,  $\gamma_{\parallel}$  is smaller than  $\gamma_{\perp}$ ,<sup>27</sup> and consequently a larger diffusion coefficient along  $X_{\parallel}$  axis than along  $Y_{\perp}$  axis is expected if a particle's rotation is prohibited. Such anisotropic motion is also valid for a short time when rotation is allowed.<sup>28</sup> We resolved this behavior by decomposing the rod's displacement into components relative to the body frame [ $X_{\parallel}, Y_{\perp}$ ] or the lab frame [ $x, y, \theta$ ]. As shown in Figure 3C, their relation can be expressed as  $X_{\parallel} = \Delta x \cos \theta + \Delta y \sin \theta$  and  $Y_{\perp} = -\Delta x \sin \theta + \Delta y \cos \theta$ , where  $\Delta x = (x_1 - x_2)$ ,  $\Delta y = (y_1 - y_2)$ , and  $\theta = \theta_1$ . We calculated the mean-square displacement (MSD) vs time ( $t$ ) along  $X_{\parallel}$  and  $Y_{\perp}$  axes (Figure 3D) and obtained the anisotropic diffusion coefficients of  $0.26 \text{ nm}^2/\text{s}$  along the  $X_{\parallel}$  axis and  $0.16 \text{ nm}^2/\text{s}$  along the  $Y_{\perp}$  axis (estimated from the slope of the plots). The histograms of the displacement distribution along the two axes show a larger deviation corresponding to a larger diffusion coefficient along the  $X_{\parallel}$  axis (Figure 3E). The detailed evolution of the rod trajectory from short-term anisotropic motion to long-time isotropic motion due to the rod rotation can be further resolved.

When following the behavior of individual particles before and after the initiation of drying patches, we found distinctly different modes of motion. This is apparent from the trajectory of a 5 nm spherical particle motion through a sequence of movements in Figure 4A. The displacement ( $\lambda$ ) during a time interval ( $\Delta t$ ) vs time ( $t$ ) was analyzed (Figure 4B) using the same method as in Figure 2B. Similar behavior of the particle jumps followed by small-step movements was observed during the first 400 s of movement. Jumps corresponding to particle rolling are observed.

At the later stages of the particle movement (see Figure 4B), the motion is heavily biased. In addition, large-step displacements (also manifested as jumps in the trajectory, see Figure 4A b→c) were an order of magnitude larger than the average jump length in a liquid film at the early stage. The corresponding images elucidate that drying patches formed in the liquid film and particles were dragged by the nearby retracting liquid front (Figure 4C). Since the particle contrast does not change during these drying patch induced large jumps, we conclude that the motion proceeded primarily by sliding at this stage. Correlated jumps between nearby particles were observed in some cases, supporting the suggestion of liquid drag.

In the present study we have directly resolved the complex motion of inorganic nanoparticles in a liquid thin film during solvent evaporation. Our observations reveal three distinctly different modes of particle motion: (1) center-of-mass displacement over short length scales, (2) rolling over longer length scales, and, finally, (3) dragging by the fluid front over considerably longer distances. A combination of these three modes of movements determines the ultimate motion of the particle during the drying

process. This work has provided a unique view of the motion of individual nanoparticles during solvent evaporation, providing the necessary groundwork for future studies of correlated motion in more concentrated particle solutions and for studies of particle diffusion during self-assembly processes intended to create complex functional nanoparticle arrangements. In addition, gold nanoparticles have been used as labels for electron microscopy of frozen biological samples for decades. The work described here suggests that it may not be long before dynamical motion of biological molecules can be tracked by electron microscopy in physiological environments.

**Acknowledgment.** We gratefully acknowledge J. Ku, Professor P. L. Geissler, and Professor H. Yang for useful discussions and Dr. H. Liu and J. Turner for their help at the beginning of image processing and data analysis. S. Claridge is supported by an NSF-IGERT predoctoral fellowship. This work was performed at the National Center for Electron Microscopy, Lawrence Berkeley National Laboratory, and was supported by the Office of Science, Office of Basic Energy Sciences of the U.S. Department of Energy under Contract No. DE-AC02-05CH11231.

**Supporting Information Available:** Liquid cell fabrication, experimental details, and discussions on electron beam effects. This material is available free of charge via the Internet at <http://pubs.acs.org>.

## References

- (1) Deegan, R. D.; Bakajin, O.; Dupont, T. F.; Huber, G.; Nagel, S. R.; Witten, T. A. *Nature* **1997**, *389* (6653), 827–829.
- (2) Rabani, E.; Reichman, D. R.; Geissler, P. L.; Brus, L. E. *Nature* **2003**, *426* (6964), 271–274.
- (3) Bigioni, T. P.; Lin, X. M.; Nguyen, T. T.; Corwin, E. I.; Witten, T. A.; Jaeger, H. M. *Nat. Mater.* **2006**, *5* (4), 265–270.
- (4) Cui, Y.; Bjork, M. T.; Liddle, J. A.; Sonnichsen, C.; Boussert, B.; Alivisatos, A. P. *Nano Lett.* **2004**, *4* (6), 1093–1098.
- (5) Lin, X. M.; Jaeger, H. M.; Sorensen, C. M.; Klabunde, K. J. *J. Phys. Chem. B* **2001**, *105* (17), 3353–3357.
- (6) Granick, S. *Science* **1991**, *253* (5026), 1374–1379.
- (7) Heuberger, M.; Zach, M.; Spencer, N. D. *Science* **2001**, *292* (5518), 905–908.
- (8) Kaizuka, Y.; Groves, J. T. *Phys. Rev. Lett.* **2006**, *96* (11), 118101.
- (9) Frolov, V. A.; Klapp, S. H. L. *J. Chem. Phys.* **2006**, *124* (13), 134701.
- (10) Myers, T. G. *Siam Rev.* **1998**, *40* (3), 441–462.
- (11) Williamson, M. J.; Tromp, R. M.; Vereecken, P. M.; Hull, R.; Ross, F. M. *Nat. Mater.* **2003**, *2* (8), 532–536.
- (12) Howe, J. M.; Yokota, T.; Murayama, M. *J. Electron Microsc.* **2004**, *53* (2), 107–114.
- (13) Yokota, T.; Murayama, M.; Howe, J. M. *Phys. Rev. Lett.* **2003**, *91* (26), 265504.
- (14) Egerton, R. F.; Li, P.; Malac, M. *Micron* **2004**, *35* (6), 399–409.
- (15) Chen, C. T.; Tseng, F. G.; Chieng, C. C. *Sens. Actuators, A* **2006**, *130*, 12–19.
- (16) Raptis, T. E.; Raptis, V. E.; Samios, J. *J. Phys. Chem. B* **2007**, *111* (49), 13683–13693.
- (17) Fultz, B.; Howe, J. M. *Transmission Electron Microscopy and Diffractometry of Materials*; Springer: Berlin, 2002.
- (18) Bardotti, L.; Jensen, P.; Hoareau, A.; Treilleux, M.; Cabaud, B.; Perez, A.; Aires, F. C. S. *Surf. Sci.* **1996**, *367* (3), 276–292.
- (19) Naumovets, A. G.; Zhang, Z. Y. *Surf. Sci.* **2002**, *500* (1–3), 414–436.
- (20) Sonnichsen, C.; Alivisatos, A. P. *Nano Lett.* **2005**, *5* (2), 301–304.
- (21) Luedtke, W. D.; Landman, U. *Phys. Rev. Lett.* **1999**, *82* (19), 3835–3838.
- (22) Shlesinger, M. F.; Zaslavsky, G. M.; Klafter, J. *Nature* **1993**, *363* (6424), 31–37.

- (23) Chechkin, A. V.; Klafter, J.; Gonchar, V. Y.; Metzler, R.; Tanatarov, L. V. *Phys. Rev. E* **2003**, *67* (1), 010102.
- (24) Lopez, M.; Graham, M. D. *Phys. Fluids* **2007**, *19* (7), 073602.
- (25) Yamaki, M.; Higo, J.; Nagayama, K. *Langmuir* **1995**, *11* (8), 2975–2978.
- (26) Bestehorn, M.; Neuffer, K. *Phys. Rev. Lett.* **2001**, *87* (4), 046101.
- (27) Happel, J.; Brenner, H. *Low Reynolds Number Hydrodynamics*; Kluwer and Dordrecht: Netherlands, 1991.
- (28) Han, Y.; Alsayed, A. M.; Nobili, M.; Zhang, J.; Lubensky, T. C.; Yodh, A. G. *Science* **2006**, *314* (5799), 626–630.

NL9012369